Nuclear Instruments and Methods in Physics Research B 268 (2010) 1781–1785

Contents lists available at ScienceDirect

Nuclear Instruments and Methods in Physics Research B

journal homepage: www.elsevier.com/locate/nimb

Energy loss of protons in carbon nanotubes: Experiments and calculations

I. Kyriakou [a], C. Celedón [b], R. Segura [c,d], D. Emfietzoglou [a], P. Vargas [b], J.E. Valdés [b,c], I. Abril [e], C.D. Denton [e], K. Kostarelos [f], R. Garcia-Molina [g,*]

[a] Medical Physics Lab., University of Ioannina, Ioannina 451 10, Greece
[b] Atomic Collisions Laboratory, Physics Department, UTFSM, Valparaíso 2390123, Chile
[c] Centro de Nanociencia de Valparaíso, UTFSM, Valparaíso 2390123, Chile
[d] Departamento de Química y Bioquímica, Universidad de Valparaíso, Chile
[e] Departament de Física Aplicada, Universitat d'Alacant, Apartat 99, E-03080 Alacant, Spain
[f] Nanomedicine Lab., University of London, London WC1N 1AX, UK
[g] Departamento de Física – CIOyN, Universidad de Murcia, Apartado 4021, E-30080 Murcia, Spain

ARTICLE INFO

Article history:
Available online 26 February 2010

Keywords:
Energy loss function
Dielectric formalism
Carbon nanotubes
Energy loss and stopping power
Proton beams

ABSTRACT

We have studied the energy loss of protons in multi-walled carbon nanotube (MWCNT) samples, both experimentally and theoretically. The experiments were done in transmission geometry, using 6 and 10 keV proton beams, with the MWCNT targets dispersed on top of a ~20 nm-thick holey carbon coated TEM grid (amorphous carbon film, a-C). The energy loss of protons interacting with the MWCNTs and the amorphous carbon film is obtained after analyzing the signals coming from both types of carbon allotropes. The electronic energy loss of protons is calculated using the dielectric formalism, with the target energy loss function built from optical data. Comparison of experimental and theoretical data indicates that model calculations appropriate for three-dimensional (bulk) targets substantially overestimate the energy loss to MWCNTs. In contrast, a recent parameterization of the dielectric function of MWCNTs predicts significantly lower stopping power values compared to the bulk models, which is more in line with the present experimental data when considering the additional stopping mechanisms that are effective in the keV range.

1. Introduction

Since their discovery by Iijima in 1991 [1], carbon nanotubes (CNTs) have attracted the interest of researchers in many fields due to their outstanding mechanical and electrical properties [2]. For example, one of their most intriguing property is that despite their lightness they exhibit an exceptionally high Young modulus and tensile strength (e.g. 10–50 times those of steel), which gives them great potentials as composites and re-enforcements [3]. CNTs can also be either metals or semiconductors with a variable band-gap depending on their structure (i.e. diameter, chirality...) that along with their inherent nanometer size, makes them ideal candidates for future nanoelectronics [3]. There are of course many other properties (e.g. chemical stability) that render CNTs potentially useful over a broad spectrum of disciplines [3]. However, several issues must be addressed before their industrial use since, presently, their large-scale production seems to severely compromise many of their interesting properties. For example, it is well-known that during growth CNTs aggregate into bundles with a reduced (by a factor of 10) Young modulus due to the weak van der Waals forces among individual tubes which render them particularly prone to intertube sliding [4]. Another problem is our inability so far to control CNTs chirality during production resulting in a sizeable fraction (~30%) being metallic and, therefore, unsuitable for use as field-effects-transistors (FETs) in integrated circuits [5].

It is by now well established that both electron and ion beams offers a convenient tool for modifying CNTs structure and properties in a controllable manner with near atomic precision [6]. Ion beams have been shown to effectively thin, slice, and weld CNTs at precise locations [7], induce links between individual tubes [8] or between CNTs and substrates [9], change their electrical properties [10], or generate defects [11] which may alter their structure [12] and mediate chemical functionalization [13]. The latter effect can be particularly important in biomedical applications since pristine CNTs are known to be insoluble in most solvents (including biological) whereas, if chemically functionalized they can easily penetrate within cells and thus act as novel delivery vehicles of molecules or radionuclides [14].

Optimizing the use of ion beams requires that the rate at which energetic charged particles deposit energy in a CNT target is quantitatively determined. Although studies on slow ions effects on nanostructures where nuclear stopping (i.e. elastic scattering by

* Corresponding author. Tel.: +34 868887389; fax: +34 86 8888568.
E-mail address: rgm@um.es (R. Garcia-Molina).

0168-583X/$ - see front matter © 2010 Elsevier B.V. All rights reserved.
doi:10.1016/j.nimb.2010.02.073

target nuclei) prevails [15] are perhaps more represented in the literature (especially in the early days), there is currently increased interest for the effects of electronic stopping (i.e. inelastic scattering by target electrons) because of: (i) the expected use of CNTs in outer space [9] where high energy protons and heavier ions are abundant, (ii) the realization that, along with knock-on (elastic) atom displacement, electronic excitations might also be useful for tailoring CNTs properties since their effects are generally less destructive and reversible being mediated by chemical bond breakage [16], and (iii) the revised role of electronic excitations in mediating ionic interactions even in the low-energy (i.e. nuclear stopping) regime [17].

To our knowledge no detailed analysis is available on the energy loss of light ions passing through CNTs, except for very slow heavy ions in the nuclear stopping regime [15,18] and for channeling conditions [19,20]. In this work we present, for the first time energy loss measurements and calculations of protons beams through samples of multi-walled carbon nanotubes (MWCNTs), for incident energies of 6 and 10 keV. The experimental results are compared with theoretical calculations done in the dielectric framework for two different descriptions of the target energy loss function (ELF), namely, the MELF-GOS model which has proven suitable for many bulk (3D) materials [21,22], and a recent parameterization which corrects for the reduced dimensionality of CNTs [23]. We should recognize at the outset that the experimental energy range (~10 keV) is only marginally suitable for such a comparison given that energy loss mechanisms not included in the present calculations might have a sizeable contribution in this relatively low-energy range. However, it will be shown that an order-of-magnitude estimate of the additional stopping mechanisms suffices for drawing useful conclusions.

This paper is organized as follows. The experimental procedure is presented in Section 2, while the basis of theoretical calculations is outlined in Section 3. Finally the experimental and theoretical results are discussed in Section 4.

2. Experiments

Multi-walled carbon nanotube (MWCNT) samples have been prepared and characterized to perform ion energy loss measurements. The MWCNTs were synthesized by thermal chemical vapor deposition (CVD) in a horizontal tube furnace. In brief, 0.01 g of Pd(1%)/γ-Al_2O_3 catalyst was annealed up to 800 °C with a stream of Ar (200 cc/min) and H_2 (100 cc/min) and kept it at this temperature by 10 min. Then, acetylene (40 cc/min) was admitted in the furnace during 30 min at 800 °C, keeping the Ar/H_2 stream at the same rate. In such conditions acetylene is catalytically decomposed

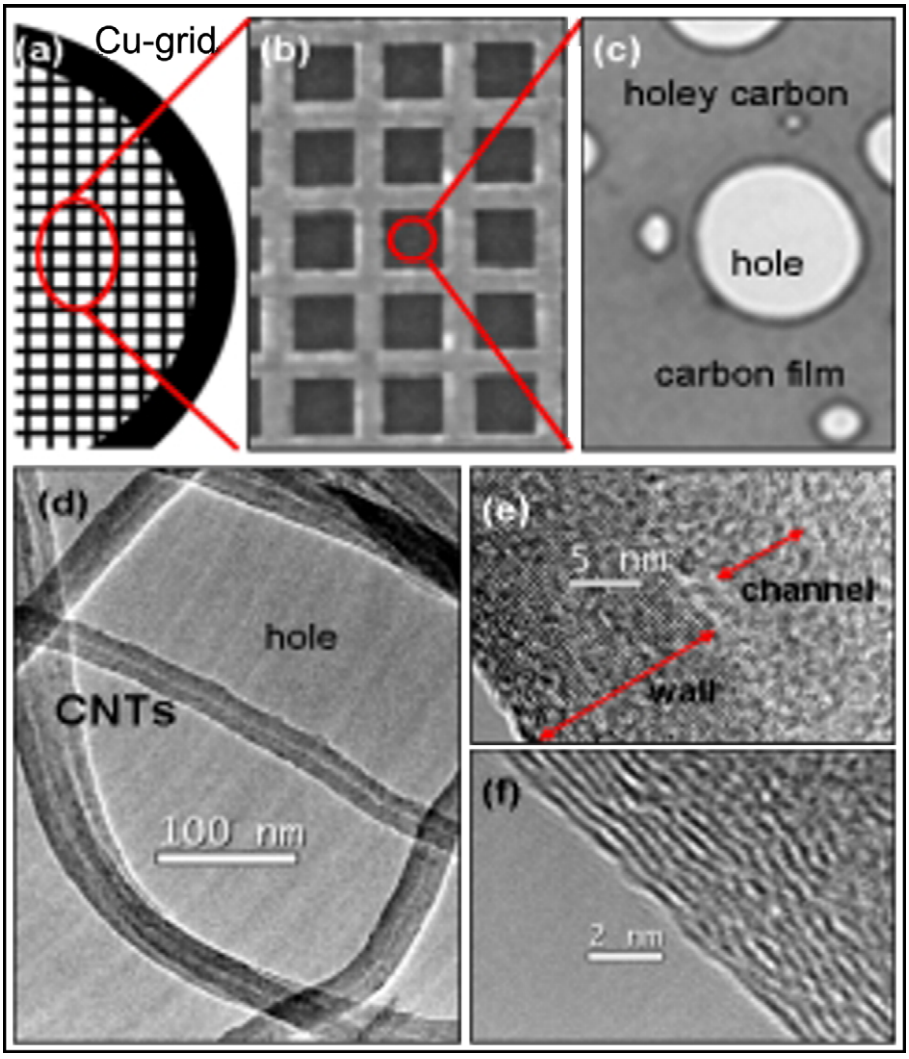

Fig. 1. Transmission electron micrographs. (a–c) Successive magnification of holey carbon supported on a copper grid. (d–f) Images of MWCNTs dispersed on holey carbon. (e–f) HRTEM images showing details about the graphitic structure of nanotubes.

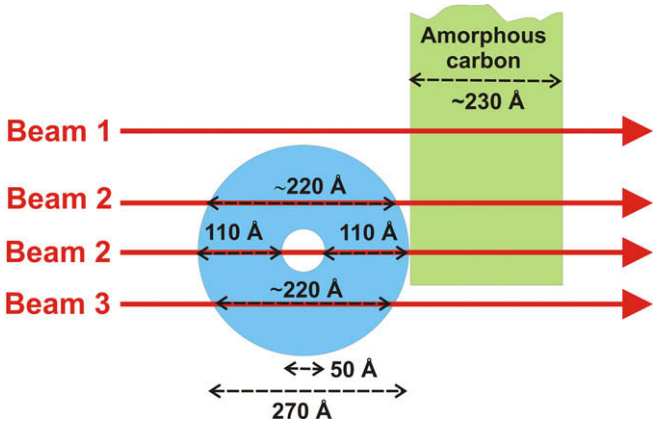

Fig. 2. Assumed layout of the MWCNT from where the energy loss were measured. Beams 1 and 3 only pass through a-C and MWCNT, respectively. Both beam labelled 2 cross the same path through MWCNT and a-C.

to yield the MWCNTs with an average diameter of 27 nm [24]. After synthesis, the samples were carefully purified by standard procedures [25] to remove the catalyst. In Fig. 1(a)–(c), we show a holey carbon coated copper grid (3 mm diameter), which is the type of sample holder used to disperse the nanotubes. Fig. 1(d)–(f) shows TEM micrographs of MWCNTs taken in a FEI Tecnai G2 F20 S-Twin microscope, operated at 200 kV. The high resolution images in Fig. 1(e) and (f) show details about the graphitic walls and the empty channel of the nanotubes. We have estimated an average inner diameter close to 5 nm.

Energy loss measurements were performed using a proton beam coming from a hot discharge ion source which is focused by an electrostatic lens system and mass selected by a Wien velocity filter. Ion energy was analyzed using a 160° spherical electrostatic analyzer with a resolution less than 1%. The associated error in the energy loss determination was less than 3%. System detection consists in a MCP detector plus electronics. The collision chamber was maintained at a pressure of 10^{-7} Torr during the experiment. The experiments were done in transmission geometry, using proton beams at 6 and 10 keV incident energies [26].

Fig. 2 shows the layout as well as the dimensions of a typical MWCNT lying on the edge of the hole of the holey carbon microgrid, which consists of amorphous carbon. The thickness of the a-C foils was estimated to be 23 nm, while the effective thickness of the MWCNTs, was taken to be 22 nm.

The experimentally determined most probable energy loss of the protons after interacting with the MWCNT and the amorphous carbon (a-C) targets are presented in Table 1, for two incident energies and different combinations of MWCNT and a-C target configurations, corresponding to the beams depicted in Fig. 2 (further details are given at the beginning of Section 4).

Table 1
Measured and calculated energy losses, ΔE_i, for two incident proton energies, for different combinations of MWCNT and amorphous carbon targets configurations (corresponding to the beams denoted by $i = 1$, 2 and 3 in Fig. 2).

	Proton incident energy = 6.02 keV			Proton incident energy = 10.1 keV		
	ΔE_1 (eV)	ΔE_2 (eV)	ΔE_3 (eV)	ΔE_1 (eV)	ΔE_2 (eV)	ΔE_3 (eV)
Experimental results	1397.6	1580.6	328.6	1648.0	2007.5	409.1
MELF-GOS calculations [21,22]	1355	1993	638	1622	2475	853
Recent parameterization calculations [23]	–	1374	19	–	1679	57

3. Theory

The stopping power of MWCNTs is calculated in the framework of the dielectric formalism [27], with the MWCNT energy loss function built from optical data in the 0–50 eV range [28] and carbon photoabsorption coefficients [29] for higher excitation energies. Two different methods are used to extend the MWCNT energy loss function to finite momentum transfers: the MELF-GOS model [21,22], and a recent parameterization of experimental CNT data on the plasmon dispersion and its linewidth broadening [23].

The stopping power S of a proton with incident energy E is calculated as the weighted average of the stopping powers for each charge-state ($q = 1$, 0) the projectile can have during its motion through the target

$$S(E) = \sum_{q=0}^{1} \phi_q(E) S_q(E). \tag{1}$$

The energy dependent projectile charge-state fractions $\phi_q(E)$ are obtained from the CasP code [30], and the corresponding projectile electronic densities are described by means of Brandt–Kitagawa statistical model [31,22].

The stopping power of a material for a swift hydrogen projectile (with charge-state q and energy E) is given by the following expression

$$S_q(E) = \frac{me^2}{\pi E} \int_0^\infty \mathrm{d}\omega\ \omega \int_{\omega/\upsilon}^\infty \frac{dk}{k} \rho_q^2(k) \mathrm{Im}\left[\frac{-1}{\varepsilon(k,\omega)}\right], \tag{2}$$

where $\upsilon = \sqrt{2E/m}$ is the projectile velocity and $\rho_q(k)$ is the Fourier transform of the projectile charge density; m and e are the electron mass and absolute charge.

The target energy loss function (ELF), $\mathrm{Im}[-1/\varepsilon(k,\omega)]$, gives the probability of producing in the target an electronic excitation with momentum $\hbar k$ and energy $\hbar\omega$; therefore, the ELF is the key parameter regarding the stopping properties of the material. Two methods are used in this paper to describe in a realistic manner the ELF of MWCNTs. Both procedures use the same fit to the measured ELF in the optical limit ($k = 0$) [28], but differ in the manner they extend the ELF to non-zero k-values.

The first one is the MELF-GOS model [21,22], which takes into account the outer-shell electron excitations through a combination of Mermin-type ELFs [32], while inner-shell electron excitations are related to the generalized oscillator strengths (GOS) of the target atoms. The extension to $k > 0$ values of the momentum transfer is automatically provided by the analytical properties of the Mermin dielectric function [32], without need of further fittings to ELF at non-zero k-values, which are scarce.

An alternative method to model the ELF at $k > 0$ is by incorporating the k-dependence directly into the Drude coefficient for the plasmon energy (ω_i) and its linewidth (γ_i). By this approach it is possible to take advantage of any available experimental data for the particular system under study. For CNTs, such data are available from k-dependent EELS measurements. We have found that the experimental data for the $\pi + \sigma$ plasmon energy and linewidth are well represented by the following dispersion relations (in a.u.) [23]:

$$\omega_i(k) = \sqrt{\omega_{i,0}^2 + \alpha k + \beta k^2 + k^4/4}, \tag{3}$$

$$\gamma_i(k) = \gamma_{i,0} + k/2 + k^2/2, \tag{4}$$

where $\alpha = \sqrt{3/10}\omega_p \upsilon_F$ and $\beta = (3/5)\upsilon_F^2$, ω_p is the plasmon energy and υ_F is the Fermi velocity of the electron gas, deduced from Ref. [28].

It is important to note that both Eqs. (3) and (4) used in Ref. [23] predict substantially different dispersion properties compared to the Mermin dielectric function, which forms the basis of the

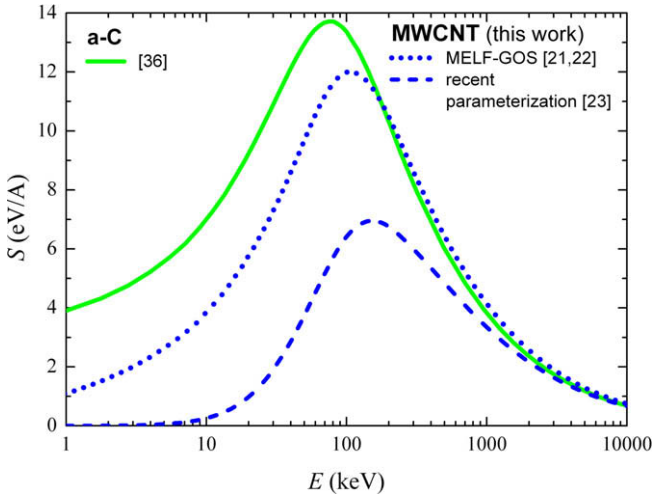

Fig. 3. Calculated stopping power of the two targets considered in this work: amorphous carbon (continuous line), and MWCNT (discontinuous lines). The former was obtained as explained in Ref. [36]; the latter was evaluated with Eqs. (1) and (2) by using the two different methods discussed in the text to extend the ELF of MWCNTs to finite momentum transfer (as indicated by the labels).

MELF-GOS model. For instance, Eq. (3) is of the same form as the plasmon dispersion relationship used by Echenique and co-workers [33], which accounts in an approximate manner for boundary effects at very low-k as well as for bulk and single-particle excitations in the intermediate and high-k range, respectively. Similarly, Eq. (4) differs from the predictions of the Mermin model [34] both with respect to the linear term and the magnitude of the quadratic coefficient.

Although the use of a macroscopic dielectric function is mostly associated with bulk or semi-infinite systems, it was recently shown to be useful even for nanostructures as long as their valence electron subsystem can be considered as a continuum [35]. This condition is expected to be valid when the plasmon energy is much larger than the band-gap and the response of the system up to relatively high excitation energies (well above the plasmon energy) is considered [35]. Both conditions are well satisfied here.

Fig. 3 depicts the stopping power of MWCNTS for protons as calculated by the dielectric formalism, Eqs. (1) and (2), when using the two different methods for constructing the ELF in the whole momentum and energy transfer space, (k, ω). The stopping power of a-C is also shown, as calculated in Ref. [36], where polarization effects [37] and electron capture-and-loss contributions to the stopping power were considered. It is worth to mention that SRIM [38] calculations for graphite (the closest target to MWCNT), sizeably exceeds the results depicted in Fig. 3.

4. Discussion

We have calculated the proton energy loss as $\Delta E_i = S_i \times \Delta x_i$, where S_i and Δx_i represent, respectively, the stopping powers (Fig. 3) and the target thicknesses crossed by the representative proton beams depicted in Fig. 2 (labelled by the subscript $i = 1$, 2 and 3). The results are shown in Table 1 as deduced from the two different theoretical schemes used for the extension of the ELF to finite momentum transfers, namely the MELF-GOS method [21,22] and the recent parameterization of the dielectric function of MWCNTs [23].

There is a remarkable agreement between the measured and calculated energy loss in a-C. However, it is clear that as compared to the experimental data, the energy loss values in MWCNTs predicted by the MELF-GOS model are too high whereas those of the parameterized model [23] are too low.

In the present experimental energy range (~10 keV) the rate of energy loss of protons is the sum of three factors, namely, the electronic stopping (S_e) due to ionization and excitation of target electrons (corrected for the changing charge-state of the projectile), the electronic stopping due to capture-and-loss (S_e^c) of electrons by the projectile, and the nuclear stopping (S_n) due to elastic collisions with the target nuclei. The calculations by either the MELF-GOS or the parameterized model refer strictly to S_e (with charge-state corrections). An estimate of S_n by the ZBL formula [39] with carbon parameters shows that in the present energy range it is only ~1–2 eV/nm. The contribution of S_e^c is more difficult to estimate but, as calculated for another low atomic number target [40], it may be of the order of 0.1 eV nm^2/atom; thus, for a density of ~100 atoms/nm^3 in MWCNTs, the S_e^c may be as large as 10 eV/nm. Clearly then, the addition of S_e^c (and S_n) will bring the calculations by the parameterized model [23] very close to the experimental data, whereas the opposite will be the case with respect to the MELF-GOS calculations.

In conclusion, the MELF-GOS model, rooted to the 3D electron gas and shown to accurately describe the excitation spectrum and stopping properties of many bulk materials (as it the case of amorphous carbon), appears less satisfactory for a MWCNT target, a prototype low dimensional system, resulting in a significant overestimation of its stopping power. In this case, it appears necessary to account, at least approximately, for surface and boundary effects as described in Ref. [23]. Differences between the stopping power values obtained form the parameterized model [23] and the experimental data could be provisionally attributed to stopping mechanisms not considered here (e.g. charge-exchange losses, elastic losses...) which, as discussed above, are expected to raise the theoretical values and bring them closer to the experimental ones. Although we make no claim regarding the rigor of the presented comparative analysis, the results seem to point out to substantially smaller than expected stopping power values for MWCNTs which, to a first approximation, can be reproduced by a simple model [23] that takes into consideration their characteristic dispersion properties which are noticeable different from those of 3D (bulk) systems. A more complete experimental study for an extended energy range from 1 to 10 keV and different carbon nanotubes sizes is under way.

Acknowledgements

This work has been financially supported by the European Union FP7 ANTICARB (HEALTH-F2-2008-201587), Financiamiento Basal para Centros Científicos y Tecnológicos de Excelencia, CEDENA, FONDECYT Grants 1071075, 1070224 and 7070175, Grant USM-DGIP 11.04.23, CONICYT/Programa Bicentenario de Ciencia y Tecnología (CENAVA) PBCTACT027, Millennium Scientific Initiative and the Spanish Ministerio de Ciencia e Innovación (Projects FIS2006-13309-C02-01 and FIS2006-13309-C02-02). CDD thanks the Spanish Ministerio de Educación y Ciencia and Generalitat Valenciana for support under the Ramón y Cajal Program.

References

[1] S. Iijima, Nature 354 (1991) 56.
[2] M.S. Dresselhaus, G. Dresselhaus, P. Avouris (Eds.), Carbon Nanotubes, Synthesis, Structure, Properties and Applications, Springer, Berlin, 2001.
[3] R.H. Bauchman, A.A. Zakhidov, W.A. de Heer, Science 297 (2002) 787.
[4] J.-P. Salvetat, G.A.D. Briggs, J.-B. Bonard, R.R. Bacsa, A.J. Kulik, T. Stockli, N.A. Burnham, L. Forro, Phys. Rev. Lett. 82 (1999) 944.
[5] P.G. Collins, P. Avouris, Sci. Am. 283 (2000) 62.
[6] A.V. Krasheninnikov, F. Banhart, Nat. Mater. 6 (2007) 723.
[7] M.S. Raghuveer, P.G. Ganesan, J. D'Arcy-Gall, G. Ramanath, M. Marshall, I. Petrov, Appl. Phys. Lett. 84 (2004) 4484.
[8] A.V. Krasheninnikov, K. Nordlund, Nucl. Instrum. Methods B 216 (2004) 355.
[9] P.P. Neupane, M.O. Manasreh, B.D. Weaver, R.P. Rafaelle, B.J. Landi, Appl. Phys. Lett. 86 (2005) 221908.

[10] B.Q. Wei, J. D'Arcy-Gall, P.M. Ajayan, G. Ramanath, Appl. Phys. Lett. 83 (2004) 3581.
[11] E. Salonen, A.V. Krasheninnikov, K. Nordlund, Nucl. Instrum. Methods B 193 (2002) 603.
[12] V.A. Basiuk, K. Kobayashi, T. Kaneko, Y. Negishi, E.V. Basiuk, J.-M. Saniger-Blesa, Nano Lett. 2 (2002) 789.
[13] B. Khare, M. Meyyappan, M.H. Moore, P. Wilhite, H. Imanaka, B. Chen, Nano Lett. 3 (2003) 643.
[14] L. Lacerda, S. Raffa, M. Prato, A. Bianco, K. Kostarelos, Nano Today 2 (2007) 38.
[15] J. Pomoell, A.V. Krasheninnikov, K. Nordlund, J. Keinonen, Nucl. Instrum. Methods B 206 (2003) 18.
[16] S. Suzuki, Y. Kobayashi, J. Phys. Chem. C 111 (2007) 4524.
[17] A.V. Krasheninnikov, Y. Miyamoto, D. Tomanek, Phys. Rev. Lett. 99 (2007) 016104.
[18] J. Pomoell, A.V. Krasheninnikov, K. Nordlund, J. Keinonen, J. Appl. Phys. 96 (2004) 2864.
[19] C.S. Moura, L. Amaral, J. Chem. Phys. B 109 (2005) 13515.
[20] Z.L. Mišković, J. Phys.: Conf. Ser. 133 (2008) 012011.
[21] I. Abril, R. Garcia-Molina, C.D. Denton, F.J. Pérez-Pérez, N.R. Arista, Phys. Rev. A 58 (1998) 357.
[22] S. Heredia-Avalos, R. Garcia-Molina, J.M. Fernández-Varea, I. Abril, Phys. Rev. A 72 (2005) 052902.
[23] I. Kyriakou, D. Emfietzoglou, R. Garcia-Molina, I. Abril, K. Kostarelos, Appl. Phys. Lett. 94 (2009) 263113.
[24] R.A. Segura, A. Tello, G. Cárdenas, P. Häberle, Phys. Stat. Sol. (a) 204 (2007) 513.
[25] K. Balasubramanian, M. Burghard, Small 1 (2005) 180.
[26] C. Celedón, N.R. Arista, J.E. Valdés, P. Vargas, Microelectron. J. 39 (2008) 1358. and references therein.
[27] J. Lindhard, K. Dan. Vidensk. Selsk. Mat.-Fys. Medd. 28 (8) (1954).
[28] R. Kuzuo, M. Terauchi, M. Tanaka, Jpn. J. Appl. Phys. 31 (1992) L1484.
[29] FFAST Database of NIST <http://physics.nist.gov/ffast>.
[30] P.L. Grande, G. Schiwietz, CasP. Convolution Approximation for Swift Particles, Version 3.1, 2005. Available from: <http://www.hmi.de/people/schiwietz/casp.html>.
[31] W. Brandt, M. Kitagawa, Phys. Rev. B 25 (1982) 5631.
[32] N.D. Mermin, Phys. Rev. B 1 (1970) 2362.
[33] P.M. Echenique, R.H. Ritchie, N. Barberan, J. Inkson, Phys. Rev. B 23 (1981) 6486.
[34] K. Sturm, Adv. Phys. 31 (1982) 1.
[35] N. Zabala, E. Ogando, A. Rivacoba, F.J. Garcia de Abajo, Phys. Rev. B 64 (2001) 205410.
[36] R. Garcia-Molina, I. Abril, C.D. Denton, S. Heredia-Avalos, Nucl. Instrum. Methods Phys. Res. B 249 (2006) 6.
[37] S. Heredia-Avalos, R. Garcia-Molina, Nucl. Instrum. Methods Phys. Res. B 193 (2002) 15.
[38] J.F. Ziegler, J.P. Biersack, SRIM. The Stopping and Range of Ions in Matter Version 2008. Available from: <http://www.srim.org>.
[39] M. Nastasi, J.W. Mayer, J.K. Hirvonen, Ion–solid Interactions: Fundamentals and Applications, Cambridge University Press, Cambridge, 1996 (Chapter 5).
[40] M. Dingfelder, M. Inokuti, H.G. Paretzke, Radiat. Phys. Chem. 59 (2000) 255.